PHYSICAL REVIEW FLUIDS **7**, 044608 (2022)

Closure modeling in near-wall region of steep resolution variation for partially averaged Navier-Stokes simulations

Chetna Kamble [*] and Sharath Girimaji
Department of Ocean Engineering, Texas A&M University, College Station, Texas 77843, USA

Pooyan Razi
General Motors, Warren, Michigan 48092, USA

Pedram Tazraei
Convergent Science, Madison, Wisconsin 53719, USA

Stefan Wallin
FLOW, Department of Engineering Mechanics, KTH, Stockholm 11428, Sweden

(Received 2 May 2021; accepted 21 March 2022; published 29 April 2022)

We seek to develop a closure model to enable scale-resolving simulation (SRS) of a turbulent flow to optimally switchover from a Reynolds-averaged Navier-Stokes (RANS) calculation at the wall to a specified degree of resolution in the wake or free-stream region. The closure model is derived by (i) using the physical principle that the total energy of resolved and unresolved scales should be conserved in the switchover region and (ii) establishing consistency with equilibrium boundary layer scaling of the partially resolved field. The model development is performed in the context of a partially averaged Navier-Stokes (PANS) scale-resolving method by quantifying and modeling the commutation terms resulting from varying resolutions in the wall-normal direction. The resulting wall-modeled PANS (WM-PANS) is used to compute the turbulent channel flow in the Re_τ range $180-8000$. The influence of the RANS-SRS switchover location on the computed flow field is examined. It is then demonstrated that the mean flow is reproduced with reasonable accuracy at modest computational effort without discernible log-layer mismatch even at the highest Reynolds number considered. While the Reynolds stresses are also recovered accurately over most of the flow domain, a noticeable computational transition from RANS to unsteady SRS flow behavior is observed and the underlying physics is examined. Irrespective of the location of computational transition, the unsteady features of the flow away from the wall are well captured. It is demonstrated that the proposed closure is able to inject the appropriate amount of resolved turbulence without the need for artificially generated synthetic turbulence. Overall, WM-PANS presents an accurate and computationally viable option for scale-resolving computations of near-wall high-Reynolds number flows.

DOI: 10.1103/PhysRevFluids.7.044608

I. INTRODUCTION

Steep spatial changes of flow features in the near-wall region render direct numerical simulations (DNS) of turbulent boundary layers computationally prohibitive at high Reynolds numbers. Even

[*]Corresponding author: chetna_2491@tamu.edu

wall-resolved large-eddy simulations (WR-LES) can be very expensive in the Reynolds number range of most boundary layers in practical flows [1]. At the other extreme of the closure modeling spectrum, Reynolds-averaged Navier-Stokes (RANS) models capture the mean-flow and turbulent shear stress profiles accurately [2] at a very modest computational cost. The qualified success of RANS models is due to the fact that important closure coefficients are derived based on equilibrium boundary layer (EBL) scaling laws. Thus motivated, many authors have attempted to adapt EBL analysis for obtaining accurate subgrid wall closures for LES [3–7]. The resulting methods, called wall-modeled LESs (WM-LESs), have less stringent resolution requirements near the wall and yield reasonable results.

Aside from LES, other scale-resolving simulation (SRS) methods have emerged over the last two decades. The SRS approaches can be broadly divided into two main groups: zonal and bridging methods [8]. In zonal methods, different turbulence models (e.g., RANS and LES in Ref. [9]) are used at different predefined locations in the domain. The energy exchange between the two turbulence models is usually achieved by introducing synthetic turbulence at the interface. Bridging or seamless methods [10], on the other hand, can automatically switch between the RANS and LES modes while accommodating scale-dependent physics. The interface between RANS and LES regions is variously called grey area, hand-shake region, switchover zone, etc. One of the enduring challenges in the bridging methods approach is to model the switchover region in a physically reasonable manner.

As in the case of LES, near-wall computation of some SRS methods (e.g., Refs. [11,12]) can employ either wall-resolved (WR-SRS) or wall-modeled (WM-SRS) strategies. In WR-SRS, the degree of flow resolution is nearly uniform throughout the flow domain. As in WR-LES, the computational burden of WR-SRS can be significant. For computational expediency, WM-SRS seeks to emulate RANS behavior near the wall and then smoothly switchover to a scale-resolving computation in the interior of the domain. In both LES and SRS, the wall-modeling strategy transfers the burden from large computational effort to higher fidelity closure models in the near-wall region.

The objective of this paper is to develop a near-wall closure model to enable accurate and computationally viable WM-SRS. The study involves three distinct steps: (i) closure model development in the switchover region, (ii) examination of the effect of commutation residue in the switchover region on the simulated flow physics, and (iii) assessment of WM-SRS in turbulent channel flow over Re_τ range of $180 - 8000$.

In the model development stage, we first identify the form and function of the commutation residue that arises when a spatially varying filter is applied to the Navier-Stokes equations in the switchover region. Then, the model is derived by utilizing two important physical considerations: (i) the total kinetic energy contained in the resolved and unresolved scales of motion must be invariant of the spatial changes in filter width and (ii) the EBL scalings of filtered flow fields are preserved [13]. The closure models are developed in the context of the SRS approach called the partially averaged Navier-Stokes (PANS) method [14].

This paper is organized as follows. Section II presents the PANS governing equations. Development of near-wall physics modeling of the commutation residue is performed in Sec. III. Section IV contains a brief description of the numerical method for implementing WM-SRS. The results are presented in Sec. V, and the paper concludes in Sec. VI with a summary.

II. GOVERNING EQUATIONS OF PANS

The velocity and pressure fields in an incompressible flow field are governed by the conservation of mass (continuity) and momentum (Navier-Stokes) equations:

$$\frac{\partial V_i}{\partial t} + V_j \frac{\partial V_i}{\partial x_j} = -\frac{\partial p}{\partial x_i} + \nu \frac{\partial^2 V_i}{\partial x_j \partial x_j}, \tag{1}$$

$$\frac{\partial V_i}{\partial x_i} = 0; \quad \frac{\partial^2 p}{\partial x_j \partial x_j} = -\frac{\partial V_i}{\partial x_j}\frac{\partial V_j}{\partial x_i}. \tag{2}$$

Here, V_i and p represent the instantaneous velocity and pressure (with subsumed density) fields and ν is the fluid kinematic viscosity. A filter operator ($<>$) is used to decompose the velocity and pressure fields into the resolved and unresolved parts [15]:

$$V_i = U_i + u_i,\ U_i = \langle V_i \rangle,\ \langle u_i \rangle \neq 0, \tag{3}$$

$$p = P + p_u,\ P = \langle p \rangle,\ \langle p_u \rangle \neq 0. \tag{4}$$

In general, the filtering operator ($<>$) is noncommutative, i.e., it may not commute with the spatial and temporal derivatives. Applying the spatiotemporal filter to the Navier-Stokes equations, the resolved field takes the form [16]

$$\frac{\partial U_i}{\partial t} + U_j \frac{\partial U_i}{\partial x_j} = -\frac{\partial \tau(V_i, V_j)}{\partial x_j} - \frac{\partial P}{\partial x_i} + \nu \frac{\partial^2 U_i}{\partial x_j \partial x_j} - F_i, \tag{5}$$

$$\frac{\partial^2 P}{\partial x_i \partial x_i} = -\frac{\partial U_i}{\partial x_j}\frac{\partial U_j}{\partial x_i} - \frac{\partial^2 \tau(V_i, V_j)}{\partial x_i \partial x_j} - \frac{\partial F_i}{\partial x_i}. \tag{6}$$

where $\tau(V_i, V_j)$ is the generalized subfilter stress (SFS) introduced in Germano [15] and F_i is the commutation residue term.

The commutation residue term, F_i in Eqs. (5) and (6) is given by Girimaji and Wallin [16] as

$$F_i = \left\langle \frac{\partial V_i}{\partial t} \right\rangle + \left\langle V_j \frac{\partial V_i}{\partial x_j} \right\rangle + \left\langle \frac{\partial p}{\partial x_i} \right\rangle - \left\langle \nu \frac{\partial^2 V_i}{\partial x_j \partial x_j} \right\rangle \\ - \frac{\partial U_i}{\partial t} - U_j \frac{\partial U_i}{\partial x_j} - \frac{\partial P}{\partial x_i} + \nu \frac{\partial^2 U_i}{\partial x_j \partial x_j} - \frac{\partial \tau(V_i, V_j)}{\partial x_j}. \tag{7}$$

When the filter is commutative, $F_i = 0$ and nonzero otherwise. In general, slow changes in physical resolution do not incur much commutation residue ($F_i \approx 0$) and uniform-resolution closure models can be used. However, if the resolution variation in the switchover region is steep, the commutation residue can be dominant and its effect must be suitably modeled [16,17].

The generalized second moment of velocity field or SFS is given by [15]

$$\tau(V_i, V_j) = \langle V_i V_j \rangle - \langle V_i \rangle \langle V_j \rangle. \tag{8}$$

In principle, the SFS can be modeled at different levels similar to the closure of Reynolds stress. In its simplest form, SFS can be modeled via the Boussinesq approximation [14,18],

$$\tau(V_i, V_j) = -2\nu_u S_{ij} + \frac{2}{3} k_u \delta_{ij}, \quad \text{where} \quad \nu_u = \frac{k_u}{\omega_u}, \tag{9}$$

where ν_u, k_u, and ω_u are the unresolved eddy viscosity, unresolved kinetic energy, and unresolved specific dissipation rate, respectively. S_{ij} is the resolved strain-rate tensor defined as

$$S_{ij} = \frac{1}{2}\left(\frac{\partial U_i}{\partial x_j} + \frac{\partial U_j}{\partial x_i}\right). \tag{10}$$

In PANS, the filter (or partition) between the resolved and unresolved field is enforced implicitly through the specification of the ratios of unresolved-to-total kinetic energy and dissipation rate (or a suitable surrogate). These ratios are defined as

$$f_k \equiv \frac{k_u}{k}, \quad f_\varepsilon \equiv \frac{\varepsilon_u}{\varepsilon}, \tag{11}$$

where k is the total kinetic energy and ε_u and ε are the unresolved and total turbulent dissipation rates. The unresolved kinetic energy and dissipation rate are obtained from the modeled evolution equations. It is evident that the two limiting cases of SRS are RANS ($f_k = f_\varepsilon = 1$) and DNS ($f_k \rightarrow$

0, $f_\varepsilon \to 0$). For intermediate values of these parameters, flow fields of differing degrees of resolution can be obtained.

The governing equations for PANS $k_u - \omega_u$ model take the following form [18]:

$$\frac{\partial k_u}{\partial t} + U_j \frac{\partial k_u}{\partial x_j} = P_u - \beta^* k_u \omega_u + \frac{\partial}{\partial x_j}\left[(\nu + \nu_u/\sigma_{ku})\frac{\partial k_u}{\partial x_j}\right], \tag{12}$$

$$\frac{\partial \omega_u}{\partial t} + U_j \frac{\partial \omega_u}{\partial x_j} = \alpha \frac{\omega_u}{k_u} P_u - \beta' \omega_u^2 + \frac{\partial}{\partial x_j}\left[(\nu + \nu_u/\sigma_{\omega u})\frac{\partial \omega_u}{\partial x_j}\right], \tag{13}$$

where the unresolved eddy viscosity (ν_u) is determined from Eq. (9). Throughout this paper, the subscript u denotes the unresolved quantities. The parameters σ_{ku} and $\sigma_{\omega u}$ are the transport coefficients of the modeled turbulent kinetic energy and specific dissipation rate. The values of the RANS closure coefficients in Eqs. (12) and (13) are $\beta^* = 0.09$, $\alpha = 5/9$, $\beta = 0.075$, $\sigma_k = 2.0$, and $\sigma_\omega = 2.0$. β' is the scale-dependent model coefficient which is obtained from [18]

$$\beta' = \alpha\beta^* - \alpha\frac{\beta^*}{f_\omega} + \frac{\beta}{f_\omega}, \text{ where } f_\omega = \frac{f_\epsilon}{f_k}. \tag{14}$$

For the uniform-f_k case, Tazraei and Girimaji [13] developed the turbulent transport coefficients, σ_{ku} and $\sigma_{\omega u}$, using EBL analysis:

$$\sigma_{ku} = \frac{f_k}{f_\omega}\sigma_{k,\mathrm{RANS}}, \quad \sigma_{\omega u} = \frac{f_k}{f_\omega}\sigma_{\omega,\mathrm{RANS}}. \tag{15}$$

These values of σ_{ku} and $\sigma_{\omega u}$ yield correct log-layer behavior.

The grid size required for PANS computations depends on the cutoff control parameters f_k and f_ϵ. The relationship between the PANS resolution control parameters and the cutoff length scale (l_c) of the computed resolved field can be developed using the Kolmogorov turbulence scaling arguments [19],

$$l_c \sim C_\mu^{3/4}\frac{f_k^{3/2}}{f_\epsilon}L, \tag{16}$$

where $L = k^{3/2}/\varepsilon$ is the integral length scale of turbulence and $C_\mu = 0.09$. Clearly, the cutoff length scale (l_c) must be larger than the grid resolution (Δ) [11]:

$$l_c \geqslant \Delta \quad \to \quad f_k \geqslant 3\left(\frac{\Delta}{L}\right)^{\frac{2}{3}}. \tag{17}$$

This inequality provides the relationship between physical resolution, f_k, and grid size (numerical resolution) and is true for the regions of fully developed turbulence. Throughout the paper, the term physical resolution is used to indicate the filter width implied by f_k and the numerical resolution refers to the grid size (Δ).

Thus far, PANS with spatially uniform f_k has been used to compute various canonical flows to establish the theoretical foundation [18,20–26]. Notably, using the paradigm that SRS is DNS of a non-Newtonian fluid, various aspects of Kolmogorov hypotheses have been extended to PANS fluctuating fields [19]. PANS has also been used for a variety of engineering flows [27–29]. In many of these simulations, f_k varies slowly enough to justify neglect of the commutation residue. At this stage of development, PANS is ideally positioned for extension to near-wall modeling.

III. NEAR-WALL CLOSURE MODELING

The near-wall region is characterized by the presence of steep variations of mean velocity field and small length scales. In wall-resolved PANS (WR-PANS), a constant f_k value is used at the wall and interior regions. This entails very fine resolution near the wall, rendering the calculations computationally expensive.

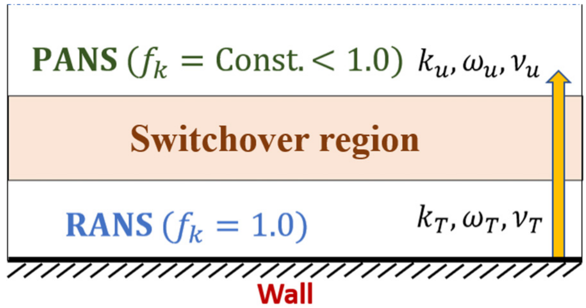

FIG. 1. RANS-SRS switchover region near the wall.

In this paper, we propose a wall-modeled PANS (WM-PANS) approach which permits f_k variation from a value of unity near the wall to a smaller value in the outer region. As the near-wall region is completely modeled using the RANS approach ($f_k = 1$), WM-PANS has significantly less stringent grid requirements. Hence, there is a compelling need for developing closure models that enable high-fidelity WM-PANS simulations.

In a typical wall-modeled SRS computation, the boundary layer is divided into three distinct computational regions as shown in Fig. 1: near-wall RANS zone of $f_k = 1$, the grey area (or the switchover region), and outer SRS region of $f_k < 1$. The simulated flow undergoes a change in description from a relatively steady flow at the wall to highly resolved unsteady flow in the outer region. Closure modeling in the switchover region represents one of the modern challenges in practical turbulent flow computations.

A. Closure modeling in region of varying f_k

As mentioned previously, in the case of varying resolution (varying f_k), the cutoff filter does not commute with spatiotemporal derivatives, leading to extra forcing terms in the governing equations. While modeling the commutation terms for temporal variation in f_k is discussed in Ref. [16], here we develop closure models of terms that arise due to a spatiotemporal variation of f_k. As in Ref. [16], the mathematical framework for these closures comes from commutation residue formulation and the physical principle emerges from the requirement that the total kinetic energy (resolved + unresolved) must be independent of changes in f_k.

We first proceed to formulate the commutation terms in the unresolved scales due to a spatiotemporally varying f_k. The unresolved scales are modeled according to the Boussinesq closure [Eq. (9)]. The unresolved kinetic energy evolution equation is derived as (see Appendix A for details)

$$\frac{\partial k_u}{\partial t} + U_j \frac{\partial k_u}{\partial x_j} = P_u - \beta^* k_u \omega_u + \frac{\partial}{\partial x_j}\left[(\nu + \nu_u/\sigma_{ku})\frac{\partial k_u}{\partial x_j}\right] + P_{\mathrm{Tr}} + D_{\mathrm{Tr}}, \tag{18}$$

where P_{Tr} is additional source term arising due to spatiotemporal variation of f_k in the advective term derived as

$$P_{\mathrm{Tr}} \equiv \frac{k_u}{f_k}\left(\frac{\partial f_k}{\partial t} + \overline{U_j}\frac{\partial f_k}{\partial x_j}\right), \tag{19}$$

where $\overline{U_j}$ is the mean velocity component. Similarly, the commutation residue due to spatial variations of f_k in the diffusion term is

$$D_{\mathrm{Tr}} \equiv -\frac{k_u}{f_k}\frac{\partial}{\partial x_j}\left(\nu_u^* \frac{\partial f_k}{\partial x_j}\right) - \frac{2\nu_u^*}{f_k}\left(\frac{\partial k_u}{\partial x_j} - \frac{k_u}{f_k}\frac{\partial f_k}{\partial x_j}\right)\frac{\partial f_k}{\partial x_j}; \quad \nu_u^* = \nu + \frac{\nu_u}{\sigma_{ku}}. \tag{20}$$

The P_{Tr} and D_{Tr} terms account for the additional energy exchange between the resolved and unresolved scales due to resolution change in the switchover region.

The specific rate of dissipation ω_u model equation for the case of uniform f_k is given in Lakshmipathy and Girimaji [30]. For the WM-PANS case, this evolution equation becomes (see Appendix B for full details):

$$\frac{\partial \omega_u}{\partial t} + U_j \frac{\partial \omega_u}{\partial x_j} = \alpha \frac{\omega_u}{k_u} P_u - \beta' \omega_u^2 + \frac{\partial}{\partial x_j}\left[(\nu + \nu_u/\sigma_{\omega u})\frac{\partial \omega_u}{\partial x_j}\right] + D_{\text{Tr}\omega}, \tag{21}$$

where the additional term, $D_{\text{Tr}\omega}$ is derived to be

$$D_{\text{Tr}\omega} = -\frac{\omega_u}{k_u}(P_{\text{Tr}} + D_{\text{Tr}}). \tag{22}$$

It is important to note that in regions of negligible f_k variation, the P_{Tr}, D_{Tr}, and $D_{Tr\omega}$ terms vanish and the k_u and ω_u equations [Eqs. (18) and (21)] revert to their corresponding uniform-f_k formulations [Eqs. (12) and (13)]. We next seek to account for the effect of varying resolution on the resolved flow field.

B. Effect of varying f_k on resolved flow field

The energy in the resolved flow field ($E_r = \frac{1}{2}U_iU_i$) can be calculated from Eq. (5) as

$$\begin{aligned} \frac{\partial E_r}{\partial t} + U_j \frac{\partial E_r}{\partial x_j} = &-\frac{\partial}{\partial x_j}(\tau(V_i, V_j)U_i) + \frac{\partial U_i}{\partial x_j}\tau(V_i, V_j) \\ &- \frac{\partial P}{\partial x_i}U_i + \nu \frac{\partial^2 E_r}{\partial x_j \partial x_j} - \nu \frac{\partial U_i}{\partial x_j}\frac{\partial U_i}{\partial x_j} - F_i U_i. \end{aligned} \tag{23}$$

The various terms on the right-hand side of Eq. (23) are turbulent transport of resolved kinetic energy, negative of resolved kinetic energy production, resolved field pressure work, viscous diffusion, and dissipation. Finally, F_iU_i represents the change in resolved energy due to the commutation residue and it plays an important role in closure modeling of the switchover region. Energy conservation requires that the commutation residue term, F_iU_i, must be balanced by the additional terms in unresolved energy equation [Eq. (18)] to precisely quantify the energy transfer between the resolved and unresolved scales.

C. Closure modeling of F_i

The forcing term F_i is responsible for the exchange of energy between unresolved and resolved scales and needs to be modeled. The first requirement on the model is the energy conservation between the resolved and unresolved scales. The variation of f_k can be seen as a variation of the computational filter scale, implying that the model should inject or remove resolved kinetic energy on the scale where the changes are active. Hence, F_i should act mainly on the smallest resolved scales.

These requirements are fulfilled by a commutation residue term, F_i, in the resolved flow equation [Eq. (5)] that is modeled as a gradient transport term [16],

$$F_i = -\frac{\partial}{\partial x_j}(2\nu_{\text{Tr}} S_{ij}), \tag{24}$$

where ν_{Tr} is termed the commutation viscosity. This commutation viscosity can be positive or negative depending upon the direction of the energy transfer [16]. Thus, the resolved flow equation, Eq. (5), can be written as

$$\frac{\partial U_i}{\partial t} + U_j \frac{\partial U_i}{\partial x_j} = -\frac{\partial P}{\partial x_i} + \frac{\partial}{\partial x_j}(2(\nu + \nu_u + \nu_{\text{Tr}})S_{ij}). \tag{25}$$

Total energy conservation dictates that $E_r + k_u$ must remain conserved independent of f_k variations. Using Eqs. (9) and (24), the evolution equation for the resolved kinetic energy (E_r) from Eq. (23) can be written as

$$\frac{DE_r}{Dt} = -\frac{\partial PU_i}{\partial x_i} + U_i\frac{\partial}{\partial x_j}(2(\nu + \nu_u + \nu_{\mathrm{Tr}})S_{ij}). \tag{26}$$

The additional viscous term in the resolved flow energy equation due to the commutation residue is decomposed as

$$U_i\frac{\partial}{\partial x_j}(2\nu_{\mathrm{Tr}}S_{ij}) = \frac{\partial}{\partial x_j}(2\nu_{\mathrm{Tr}}U_iS_{ij}) - 2\nu_{\mathrm{Tr}}S_{ij}S_{ij}. \tag{27}$$

The transport of resolved kinetic energy by the commutation term is represented by the first term on the right-hand side of Eq. (27). The second term describes the energy exchange between resolved and unresolved scales and acts mainly on the smallest resolved scales through the S^2 dependency. Using Eq. (18), the following must hold to conserve the total energy:

$$2\nu_{\mathrm{Tr}}S_{ij}S_{ij} \equiv P_{\mathrm{Tr}} + D_{\mathrm{Tr}}, \tag{28}$$

which leads to the following expression for commutation viscosity:

$$\nu_{\mathrm{Tr}} = \frac{P_{\mathrm{Tr}} + D_{\mathrm{Tr}}}{2S_{ij}S_{ij}}. \tag{29}$$

Energy transfer to the resolved scales is associated with a negative ν_{Tr}, while a positive value corresponds to energy transferred from the resolved scales to the unresolved scales. For temporal variations in f_k, Girimaji and Wallin [16] have clearly demonstrated that energy transfer in both directions is well captured by this model. Even though the total viscosity ($\nu + \nu_T + \nu_{\mathrm{Tr}}$) might take negative values resulting in a local (in time or space) exponential growth of resolved energy, the growth is limited by the available k_u and global stability can be preserved [16].

Equations (18), (21), (25), and (29), with the commutation terms derived in Eqs. (19), (20), and (22), constitute the WM-PANS model. While the formulation presented herein is in the context of PANS, the approach is applicable for all bridging SRS methods with a model transport equation representing the unresolved kinetic energy.

D. Spatial variation of physical resolution

In WM-PANS, the characteristics of the switchover region must be explicitly defined. A blending function between the RANS region and the high fidelity region away from the wall must be prescribed. A hyperbolic tangent function offers a suitable profile for a smooth f_k variation and has been widely used as a blending function in different turbulence models (e.g., DES [1], $k-\omega$ SST [31]). The following function satisfactorily describes the variation of f_k with respect to normalized wall-normal distance, y^+:

$$f_k(y^+) = a_1 - a_2\tanh\left(\frac{y^+}{\gamma} - c\right);\; a_1 = \frac{1 + f_{k(\mathrm{F})}}{2};\; a_2 = \frac{1 - f_{k(\mathrm{F})}}{2}. \tag{30}$$

Here, $f_{k(\mathrm{F})}$ is the value of f_k, i.e., the value of physical resolution in the unsteady freestream region. Parameters a_1 and a_2 are selected to ensure $f_k \approx 1$ in the RANS region close to the wall for a given $f_{k(F)}$. The constants, γ and c, control the width and location of the switchover region, respectively. Specification of these parameters for the switchover region depends on available computational resources and the required accuracy of the computed physics. It is evident that as we approach the near-wall region, $f_k(y^+) \to 1$ and Eqs. (18) and (21) reduce to the corresponding RANS equations. The influence of modifying the width (γ) and location (c) of the switchover region will be analyzed in detail in Sec. V and in the *a priori* analysis below.

TABLE I. Parameters for f_k variation for $\mathrm{Re}_\tau = 8000$: y_s^+ is the nondimensional center of the switchover region. The outer scaling values are defined as $y_s/\delta = y_s^+/\mathrm{Re}_\tau$ and $\Delta y/\delta = \gamma/\mathrm{Re}_\tau$. δ is the channel half-height.

Case	c	γ	y_s^+	y_s/δ	$\Delta y/\delta$
$A1$	3.3	60	200	2.5%	0.7%
$A2$	2.4	100	240	3.0%	1.2%
$A3$	2.0	152	288	3.6%	1.9%

E. *A priori* analysis of the switchover region

Further insight into the modeling of the commutation terms will be gained by analyzing DNS data. For this purpose, we will use the channel flow simulation [32] at $\mathrm{Re}_\tau = 8000$.

Three different cases are analyzed with different $f_k(y^+)$ profiles as presented in Table I for $\mathrm{Re}_\tau = 8000$ using the DNS data. The constants c and γ can be determined based on boundary layer scaling parameters: $y_s/\delta = y_s^+/\mathrm{Re}_\tau$ and $\Delta y/\delta = \gamma/\mathrm{Re}_\tau$, where δ is the boundary layer thickness. These values in outer scales are a better measure in wall-modeled flows as the resolution requirements are related to the boundary layer thickness. Here, $\Delta y^+ = \gamma$ is the distance over which the switchover region variation occurs.

The RANS turbulence viscosity, $\nu_{T,\mathrm{RANS}} = -\overline{uv}/(dU/dy)$, is derived from the DNS data and the unresolved quantities, k_u and ν_u, are estimated by applying the $f_k(y^+)$ function. Then, D_{Tr} is derived from Eq. (20) and ν_{Tr} from Eq. (29). The P_{Tr} term is negligible for the wall-normal f_k variation in the channel and is not considered in this analysis.

Figure 2 shows the variation of the commutation viscosity ν_{Tr} for the different cases. In addition, $\nu_{\mathrm{Tr}2}$ is evaluated as the contribution from the second term on the right-hand side of Eq. (20). ν_{Tr} is positive in the inner part of the switchover region and negative in the outer part. Hence, it will contribute to stabilizing the outer RANS region and to energizing the inner resolved region, making the transition more sharp and rapid.

The three cases show gradually smoother transition regions. A sharp switch over or transition (case A1) gives a more exaggerated behavior where the total viscosity overshoots the RANS viscosity followed by a more strong low peak. A smoother transition (case A3) gives a balanced behavior where the total viscosity well follows the RANS viscosity in the inner part. Therefore, the values of the outer scale variables (y_s/δ and $\Delta y/\delta$) corresponding to the case A3 (see Table I) should be used to obtain the parameters γ and c for WM-PANS computations at different Reynolds numbers. This will be analyzed in detail in Sec. V.

F. Flow physics in the switchover region

An analogy between the near-wall behavior of WM-PANS and DNS of a turbulent boundary layer is useful. In WM-PANS, a RANS solution is employed near the wall. In this region, high

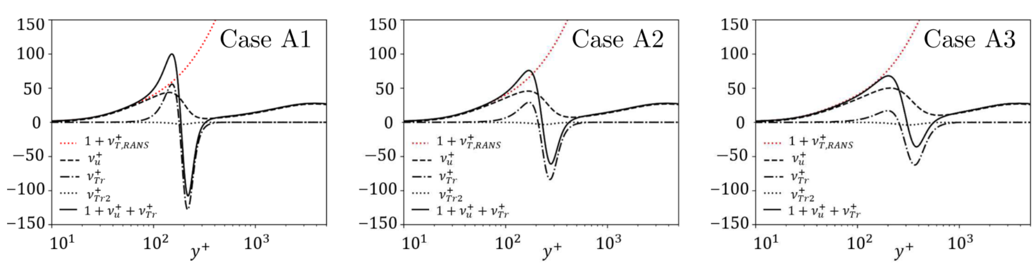

FIG. 2. *A priori* analysis of the commutation viscosity for turbulent channel flow at $\mathrm{Re}_\tau = 8000$ using DNS data [32]. The f_k variations for cases A1–A3 are presented in Table I.

effective viscosity ($\nu + \nu_t$) dampens some small-scale fluctuations. Thus, figuratively, it behaves as a computational viscous sublayer of a non-Newtonian boundary layer [19]. In simulations, however, this RANS region does exhibit some fluctuations. These are the footprints of the unsteadiness in the outer layer and have been observed in other hybrid models.

In the switchover region, the f_k value decreases below the critical value required for the instabilities to manifest. Therefore, at this location, small scales with high kinetic energy content are generated which manifest as a peak in the turbulent kinetic energy computed by WM-PANS. This behavior is similar to the physical buffer region observed in boundary layers and therefore the switchover region is characterized as a computational buffer region. This computational (or artificial) buffer-layer region analogy has also been explored in other hybrid RANS/LES turbulence models [33]. The computational buffer layer is driven by viscous instabilities similar to a natural boundary layer. The addition of the commutation viscosity, ν_{Tr}, has a significant impact. In particular, the region of negative commutation viscosity (Sec. III E) reinforces the instabilities in this region.

Finally, the high-resolution PANS region away from the wall is fully unsteady and turbulent and behaves as a computational and physical log-layer region.

In WM-PANS, the characteristics of the switchover region depend on the variation of the physical resolution (f_k). Therefore, we expect the behavior of statistics predicted by WM-PANS (including peaks in turbulent stresses) to be affected by the prescription of f_k in the domain.

The high viscosity in the RANS region near the wall dampens the formation of small resolved turbulence structures to some extent. Moreover, the high-fidelity PANS model in the region sufficiently away from the wall allows for resolution of a wide range of scales. Consequently, the switchover region between the RANS and PANS regions behaves as a computational non-turbulent/turbulent (NT/T) interface [34]. Bisset *et al.* [35] characterized this interface by a sharp change in the conditional vorticity fluctuations. Although the unsteady RANS near-wall region does resolve some fluctuations, the smaller scales are damped out. A quantitative assessment of the near-wall turbulence fluctuations is not presented in this study.

In Sec. V, we will examine the behavior of the switchover region in detail using WM-PANS for turbulent channel flow simulations for Re_τ up to 8000.

IV. SIMULATION PROCEDURE

Scale-resolved turbulent channel flow simulations are performed using an open-source finite volume code OpenFOAM [36]. Pressure-velocity coupling is achieved using a pressure-implicit with splitting of operators (PISO) [37]. Second-order accurate schemes are used for spatial and temporal discretization.

We simulate turbulent channel flow over a range of friction Reynolds numbers, $180 \leqslant \mathrm{Re}_\tau \leqslant 8000$. Periodic boundary conditions are applied in the streamwise as well as spanwise directions. The flow is driven by a constant pressure gradient in the streamwise direction. This pressure gradient is applied as a source term to the streamwise momentum equation. The algebraic equations resulting from the discretization schemes are solved using the biconjugate gradient matrix solver with a diagonal-based incomplete LU preconditioner. An iteration tolerance of 10^{-9} is specified for convergence of all variables at each time step. To ensure numerical stability, CFL is set to be less than unity. The freestream $f_{k(F)}$ (or f_k in WR-PANS) is maintained at a value of $\leqslant 0.3$ in all the simulations in this paper to ensure the underlying TS-wave instability can adequately manifest [38].

A structured mesh with hexahedral elements is employed in the domain with a uniform grid spacing in both the streamwise and spanwise directions. In the wall-normal direction, the grid cells are clustered close to the wall to obtain sufficient resolution in the near-wall region. Table II summarizes different test cases with their specific grid resolutions. It is worth noting that significantly coarse grid resolutions are utilized for the PANS (WM-PANS and WR-PANS) simulations compared to the corresponding DNS studies, particularly at high Reynolds numbers.

TABLE II. Grid resolution for turbulent channel flow simulations [Δ_x^+ and Δ_z^+ are nondimensional grid cell sizes in streamwise and spanwise directions, L_x and L_z are domain sizes in streamwise and spanwise directions; N_x, N_y and N_z denote the grid points in x, y and z directions respectively, δ is the channel half-height]; DNS values obtained from Refs. [32,39].

Re_τ	Model	N_y	Δ_x^+	Δ_z^+	L_x/δ	L_z/δ	N_x	N_z
180	PANS	101	11.2	5.6	4	2	64	64
	DNS	97	9	6.7	12π	4π		
550	PANS	101	34.2	17.1	4	2	64	64
	DNS	257	13	6.7	8π	4π	1536	1536
950	PANS	101	59.1	29.5	4	2	64	64
	DNS	385	11	5.7	8π	3π	3072	2304
2000	PANS	101	124.4	62.1	4	2	64	64
	DNS	633	12	6.1	8π	3π	6144	4608
4200	PANS	181	261.2	130.4	4	2	64	64
	DNS	1081	12.8	6.4	2π	1π		
8000	PANS	181	497.5	248.4	4	2	64	64
	DNS	4096	14.8	8.3	16	6.4	8640	6144

The *a priori* analysis of the model using DNS data (Sec. III E) shows that negative total viscosity values can be observed for WM-PANS simulations. OpenFOAM uses an implicit discretization for the viscous terms which results in numerical instabilities for negative viscosity. Hence, for stability considerations, a limiter is applied to the numerical simulations to prohibit negative values of total viscosity. While this compromises the energy exchange between the scales to some extent, the results compare reasonably well with numerical studies as presented in the next section. It should be noted, though, that local (in time or space) negative viscosity can be numerically resolved when the total kinetic energy is conserved as formulated in present modeling. This was demonstrated in Ref. [16] by applying an explicit discretization of the diffusion term in case of negative ν_{Tr}.

V. RESULTS

In this section, the necessity of near-wall modeling for high Reynolds number simulations at reasonable computational cost is first demonstrated. Next, the importance of the commutation terms for yielding the right physics in regions of varying resolution is established. Lastly, the computational effort needed to perform WM-PANS simulations for friction Reynolds numbers up to 8000 is evaluated. The results are compared to the DNS data of Hoyas and Jiménez [39] for Reynolds numbers up to 4200, and to DNS of Yamamoto and Tsuji [32] for $\mathrm{Re}_\tau = 8000$.

A. Uniform f_k simulations: WR-PANS

The mean velocity profiles for $\mathrm{Re}_\tau = 180 - 4200$ obtained from WR-PANS simulations are presented in Fig. 3. The simulations are performed at a constant $f_k = 0.2$ and the numerical resolution for different Re_τ is presented in Table II. The results clearly exhibit the ability of WR-PANS computations to adequately recover the log layer for the low Reynolds number cases ($\mathrm{Re}_\tau = 180$ and $\mathrm{Re}_\tau = 550$). However, for the higher Reynolds numbers of 2000 and 4200, the results are poor, owing to inadequate resolution of the near-wall region. In fact, at these high Reynolds numbers, the agreement with the DNS velocity profiles is restricted only to the laminar sublayer ($y^+ < 5$) and the disagreement starts early in the buffer layer.

Figure 4 illustrates the Reynolds stress profiles (streamwise, spanwise, normal, and shear) for $\mathrm{Re}_\tau = 4200$. The results indicate significant over- and underprediction of the streamwise and wall-normal WR-PANS stresses, respectively, in the near-wall region.

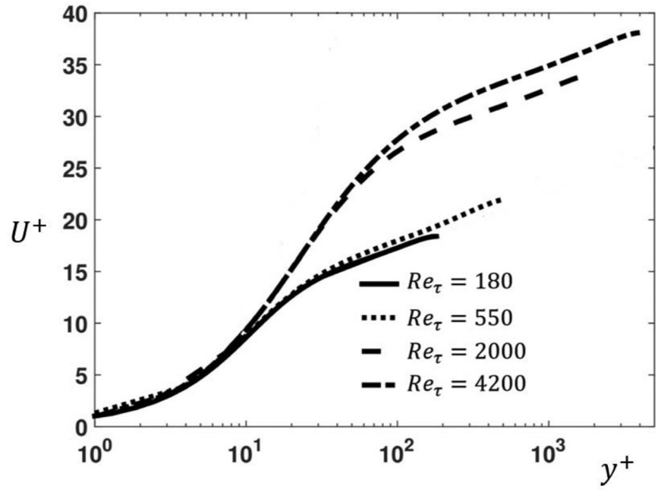

FIG. 3. WR-PANS simulation of turbulent channel flow at different Re_τ: mean streamwise velocity profile ($f_k = 0.2$).

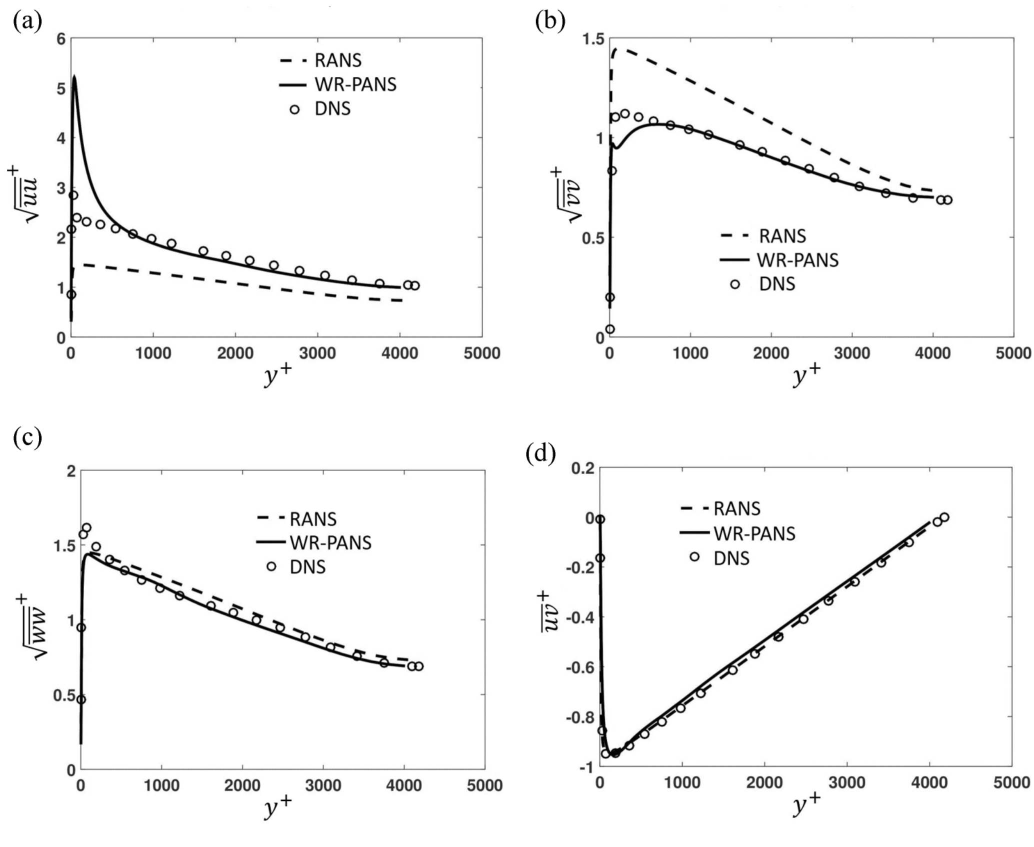

FIG. 4. WR-PANS simulation of turbulent channel flow for $\mathrm{Re}_\tau = 4200$: (a) Streamwise stress, (b) wall-normal stress, (c) spanwise stress, and (d) shear stress.

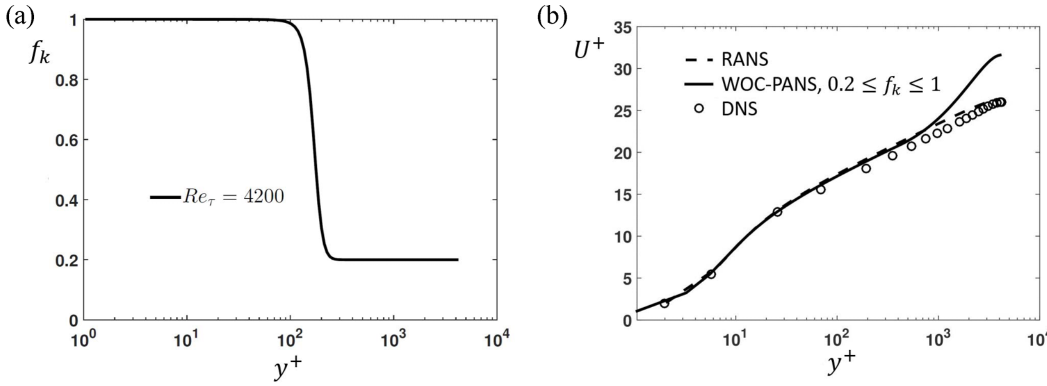

FIG. 5. WOC-PANS simulation of turbulent channel flow without the commutation terms for $\mathrm{Re}_\tau = 4200$: (a) f_k variation and (b) mean streamwise velocity.

With the current grid resolution (see Table II), WR-PANS model can capture flow physics only at relatively low Reynolds numbers ($\mathrm{Re}_\tau < 600$). For higher Reynolds numbers, substantial grid refinement is required for WR-PANS, particularly in the near-wall region for $f_k = 0.2$.

B. Variable f_k simulations without commutation terms: WOC-PANS

Now we examine the consequences of varying f_k without incorporating the corresponding commutation energy transfer terms, i.e., Eqs. (19), (20), and (22). Here, the subgrid scales are represented using the same closure models as WR-PANS, but with variable rather than a uniform f_k distribution.

Figure 5(a) shows the prescribed variation of physical resolution in the near-wall region for $\mathrm{Re}_\tau = 4200$ where f_k transitions within $100 < y^+ < 250$ based on Eq. (30). The corresponding mean velocity profile is illustrated in Fig. 5(b). The results demonstrate that solving PANS equations with varying f_k and without incorporating commutation terms (WOC-PANS), leads to an incorrect log-layer velocity gradient and a velocity overshoot in the wake. Further, as seen in Fig. 6, the turbulent stress profiles deviate significantly from the DNS results and approach the RANS solution as the flow anisotropy is not accurately captured. The results clearly demonstrate that the natural instabilities of the computational buffer layer are insufficient for obtaining the right amount

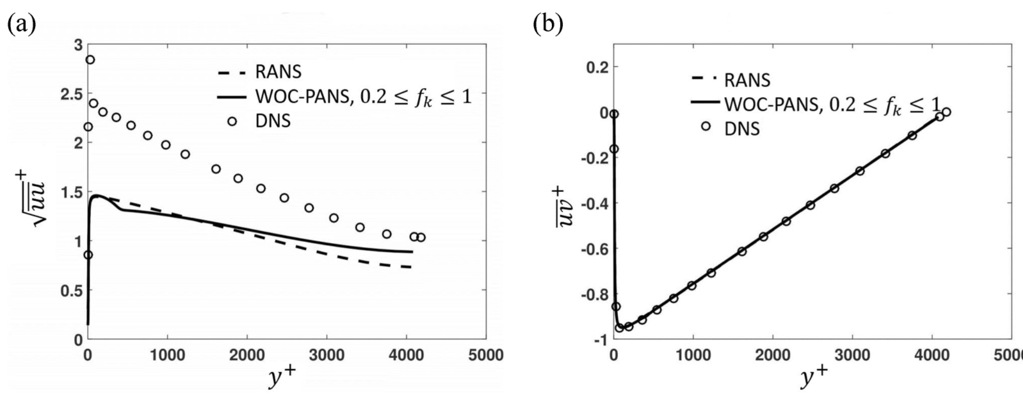

FIG. 6. WOC-PANS simulation of turbulent channel flow for $\mathrm{Re}_\tau = 4200$: (a) streamwise stress and (b) shear stress.

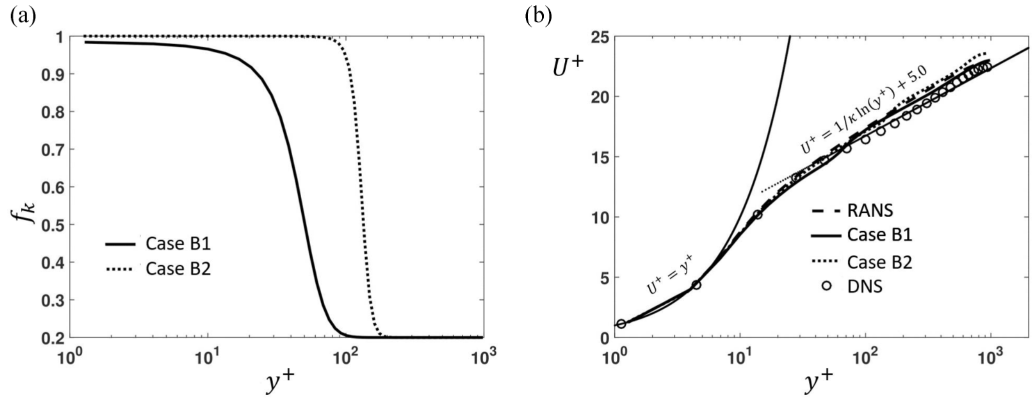

FIG. 7. (a) Prescribed f_k and (b) mean streamwise velocity profile for different cases for $\mathrm{Re}_\tau = 950$.

of resolved turbulence in the outer part. In fact, the fidelity of WOC-PANS model is even inferior to that of the under-resolved WR-PANS.

C. Variable f_k simulations with commutation terms: WM-PANS

We now present WM-PANS simulation results using variable resolution in which the commutation terms are fully accounted. For each case, the flow statistics are compared to well-documented DNS results [32,39]. We first calibrate the coefficients, c and γ, for f_k variation in the switchover region for WM-PANS. Next, we demonstrate the efficacy of WM-PANS in capturing the flow statistics in turbulent channel for $\mathrm{Re}_\tau = 950 - 8000$. Overall, in this subsection, we illustrate the effect of the switchover region (or grey area) location on the accuracy of the simulations and investigate the flow physics in this region.

1. Sensitivity to the location of the switchover region

The *a priori* analysis of the switchover region shows a smooth and well-balanced behavior of WM-PANS when $y_s/\delta \approx 3.6\%$ and $\Delta y/\delta \approx 1.9\%$ (Sec. III E). Smaller values of the outer variables (y_s/δ, $\Delta y/\delta$) can lead to larger overshoots of total viscosity, rendering the model numerically unstable. Therefore, to evaluate the sensitivity of the results to the switchover region, two different f_k variations are analyzed for $\mathrm{Re}_\tau = 950$ presented in Fig. 7(a).

For case B1 ($y_s/\delta = 3.9\%$ and $\Delta y/\delta = 2.0\%$), the resolution control parameter (f_k) transitions in the range of $20 < y^+ < 100$, whereas for the second case ($y_s/\delta = 14.2\%$ and $\Delta y/\delta = 2.1\%$), the numerical transition from RANS to PANS model occurs within $100 < y^+ < 250$. Both simulations are performed on identical grid resolutions outlined in Table II.

In turbulent channel flow, unsteadiness originates at the buffer layer and early log-layer region [40]. It is essential to resolve the underlying instabilities to accurately capture the near-wall physics. The variation of f_k for case B1 permits reasonable resolution of these instabilities whereas for case B2 these instabilities are not adequately resolved.

Figures 7(b) and 8 show the mean velocity and turbulent stress profiles for the two cases. Although case B1 is in better agreement with the DNS results, case B2 captures the first- and second-order statistics reasonably well. This is due to the consistent modeling of the commutation terms supplying the correct amount of resolved turbulence in the simulation for both cases.

In Fig. 9, isosurfaces of the second invariant of the velocity gradient tensor, Q, are presented for the two cases. As evident from the figure, a considerable amount of unsteadiness is resolved in case B1, where the f_k variation occurs in the physical buffer layer. The temporal spectra of streamwise velocity fluctuations (u) at $y^+ = 25$ and $y^+ = 500$ are presented in Fig. 10. The absence of high

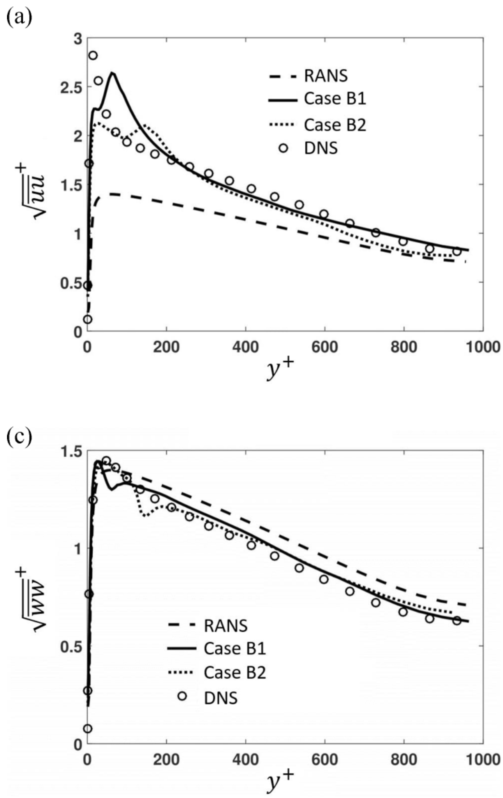

FIG. 8. WM-PANS simulation of turbulent channel flow for different cases for $\mathrm{Re}_\tau = 950$: (a) streamwise stress, (b) wall-normal stress, (c) spanwise stress, and (d) shear stress.

frequency spectral content for case B2 clearly illustrates its inability to resolve small temporal scales in the buffer region. However, in the PANS region beyond the transition location, i.e., $y^+ = 500$ [Fig. 10(b)], the temporal spectra reveal nearly identical scales for both cases, which clearly illustrate that the modeling of the commutation terms is adequate for producing real turbulence through the forcing by negative ν_{Tr}.

Overall, case B1 captures a wider range of scales and the flow structures are reasonably well resolved. Although these near-wall flow structures are not resolved in case B2, the statistics in the wake region are reasonably predicted and the associated computational effort can be substantially

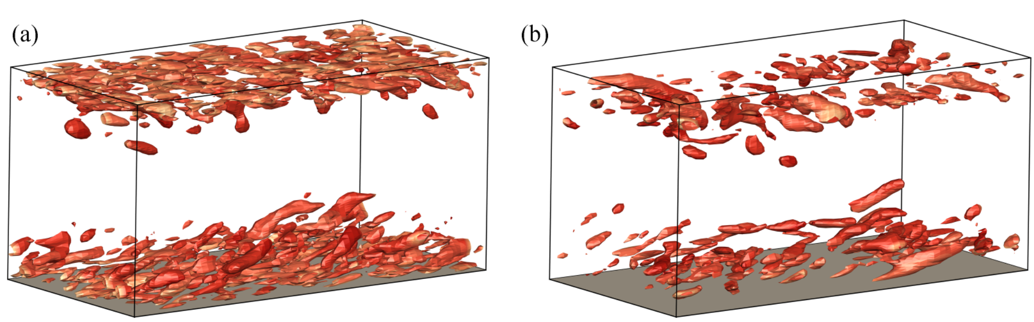

FIG. 9. Q isosurfaces (colored with streamwise velocity) (a) case B1 and (b) case B2.

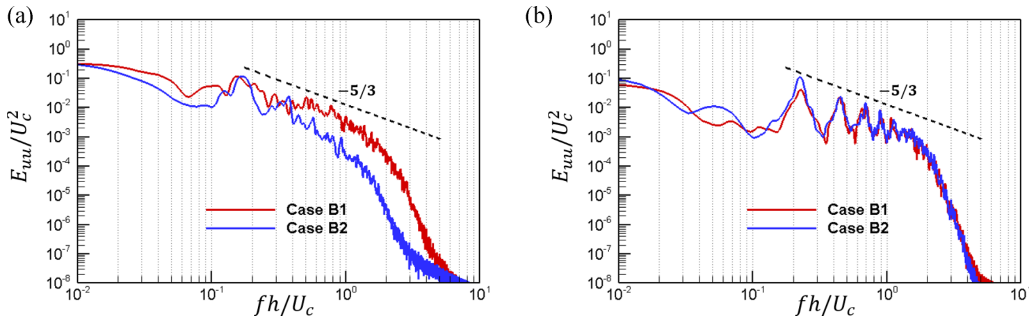

FIG. 10. Temporal spectra of streamwise velocity fluctuations for cases B1 and B2 at (a) $y^+ = 25$ and (b) $y^+ = 500$.

lower. Therefore, WM-PANS performs well when $y_s/\delta \geqslant 3.6\%$ and $\Delta y/\delta \geqslant 1.9\%$. However, large values of outer variables can reduce the fidelity of WM-PANS to effectively capture near-wall multipoint physics.

2. *WM-PANS simulations for* $\mathrm{Re}_\tau = 950 - 8000$

The objective of WM-PANS simulations is to effectively capture key unsteady features away from the wall with minimal computational effort. Toward this, we simulate the turbulent channel flow for Re_τ up to 8000 with WM-PANS based on the numerical resolution presented in Table II. The c and γ values in the f_k variation are determined based on the sensitivity analysis in the previous section. The constants for the different friction Reynolds numbers are presented in Table III. The f_k variation ensures that the viscous sublayer is fully modeled by prescribing $f_k = 1$, the transition occurs in the early log-layer region, and f_k gradually settles to a smaller value, $f_{k(F)}$, away from the wall.

In PANS simulations, a *posteriori* recovery of prescribed viscosity ratio f_ν serves as an important internal consistency check establishing the model's fidelity. The factor f_ν is defined as the ratio of the unresolved eddy viscosity to the viscosity of total fluctuations [13] and can be estimated as $f_\nu = f_k^2$. For WM-PANS, the consistency check is required to ensure that the unsteadiness in the outer region is recovered based on the prescribed freestream f_k, $f_{k(F)}$. In Fig. 11(a), recovery of f_ν is shown for the prescribed (*a priori*) f_k variation [Eq. (30)] and the constants are outlined in Table III for different Re_τ. For higher Reynolds numbers, $\mathrm{Re}_\tau = 4200$ and 8000, a negative ν_{Tr} results in a local dip in the recovery of f_k near the wall. Reasonable recovery of the filter parameter is evident in the outer region away from the wall. Clearly, the eddy viscosity ratio reaches the prescribed value ($f_{k(F)} = 0.2$) in the outer region (near-wall variation not shown). This consistency confirms that the model performs as expected, and the right level of viscosity is recovered in the solution domain.

Figure 11(b) presents the normalized mean streamwise velocity profiles at different friction Reynolds numbers. The log layer is adequately captured at all Reynolds numbers without any

TABLE III. Variation of switchover region: y_s^+ is the center of the switchover region. The outer scaling values are defined as $y_s/\delta = y_s^+/\mathrm{Re}_\tau$ and $\Delta y/\delta = \gamma/\mathrm{Re}_\tau$. δ is the channel half-height.

Case	c	γ	y_s^+	y_s/δ	$\Delta y/\delta$
$\mathrm{Re}_\tau = 950$	1.9	19	37	3.9%	2.0%
$\mathrm{Re}_\tau = 2000$	2.1	36	76	3.8%	1.8%
$\mathrm{Re}_\tau = 4200$	2.2	71	147	3.5%	1.7%
$\mathrm{Re}_\tau = 8000$	2.0	152	288	3.6%	1.9%

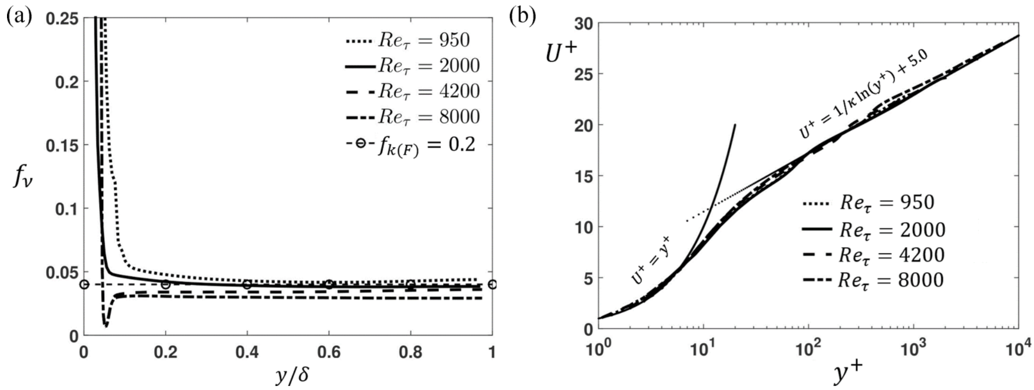

FIG. 11. WM-PANS simulation of turbulent channel: (a) Recovery of f_ν (near-wall variation of f_ν is not included) and (b) mean streamwise velocity profiles for different Re_τ.

discernible log-layer mismatch. The accuracy of WM-PANS can be attributed to the right level of energy exchange in the switchover region. It is also worth noting that the mean velocity profile for $\mathrm{Re}_\tau = 8000$ is reasonably captured with f_k distribution prescribed in Table. III. A recent DNS study of the turbulent channel flow for $\mathrm{Re}_\tau = 8000$ affirms that the logarithmic region of mean flow field is located between $300 < y^+ < 1100$ [32] and this is reasonably replicated by WM-PANS.

Profiles of turbulent stresses for the friction Reynolds number of $\mathrm{Re}_\tau = 4200$ computed from WM-PANS are presented in Fig. 12. The results are shown for freestream $f_{k(F)}$ of 0.2 and 0.3. The overall agreement of stress profiles with the DNS data is satisfactory although the deviation of streamwise stress component from the DNS results is noticeable. Further, a twitch in the total stress profiles in the switchover region is evident. The individual resolved and modeled profiles for streamwise and shear stresses are also presented in Fig. 13. The contribution of modeled stresses from RANS is significant near the wall and decreases rapidly in the outer region as more scales are resolved by the high-resolution PANS.

To better understand the behavior of turbulent stress profiles predicted by WM-PANS, we now examine the effects of the switchover location and flow physics in this region.

3. Analysis of flow behavior in the switchover region

In Fig. 12, there is a noticeable twitch in the Reynolds stress profiles coinciding with the switchover region. We investigate the underlying physics using the WM-PANS simulations of $\mathrm{Re}_\tau = 8000$ with f_k profiles presented in Table I and in Fig. 14(a). Grid resolution for the three cases is presented in Table II. These different cases represent the switch occurring progressively farther from the wall (γc) and over a wider (γ) grey zone. Figure 14(b) illustrates the streamwise Reynolds stress profiles for $\mathrm{Re}_\tau = 8000$ for different cases outlined in Fig. 14(a). From the DNS results, it is evident that the peak of the streamwise stresses occurs in the buffer region, i.e., $y^+ \approx 15$. To examine the location of WM-PANS peak, we use the paradigm that PANS is DNS of a variable viscosity fluid [19]. Accordingly, we define the effective y^+ as follows:

$$y^+_{\mathrm{eff}}(\mathrm{PANS}) = \frac{u_\tau y}{(\nu + \nu_u + \nu_{\mathrm{Tr}})}. \tag{31}$$

From Fig. 14(b), it is evident that the peak value in all cases occurs at $y^+_{\mathrm{eff}} \approx 15$. In DNS, the flow transitions naturally from buffer layer to log-layer behavior. In WM-PANS, however, this transition is forced to occur rapidly and at a location farther away from the wall dictated by the f_k prescription. In this process the commutation viscosity, ν_{Tr}, plays a key role by reducing the total viscosity thereby introducing additional instabilities, as discussed in the previous *a priori* analysis (Sec. III), enabling a rapid transition to turbulence. Therefore, the instabilities manifest in the switchover region and the

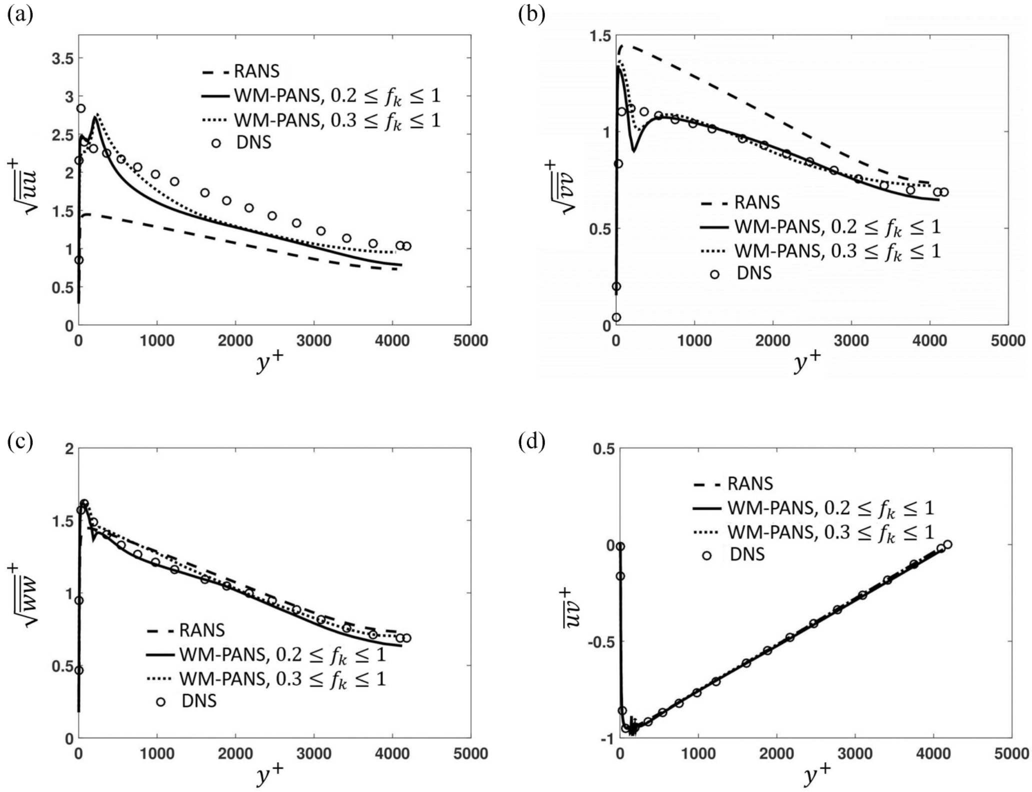

FIG. 12. WM-PANS simulation of turbulent channel for $\mathrm{Re}_\tau = 4200$: (a) streamwise stress, (b) wall-normal stress, (c) spanwise stress, and (d) shear stress.

peak values in the streamwise turbulent stresses are observed at the location of $y^+_{\text{eff}} \approx 15$. This results in a twitch in the flow statistics in the switchover region. The model recovers to the correct log-law behavior quickly. We believe that the twitch cannot be completely avoided in any switchover zone. Its effect, however, can be minimized by having a more gradual change in f_k.

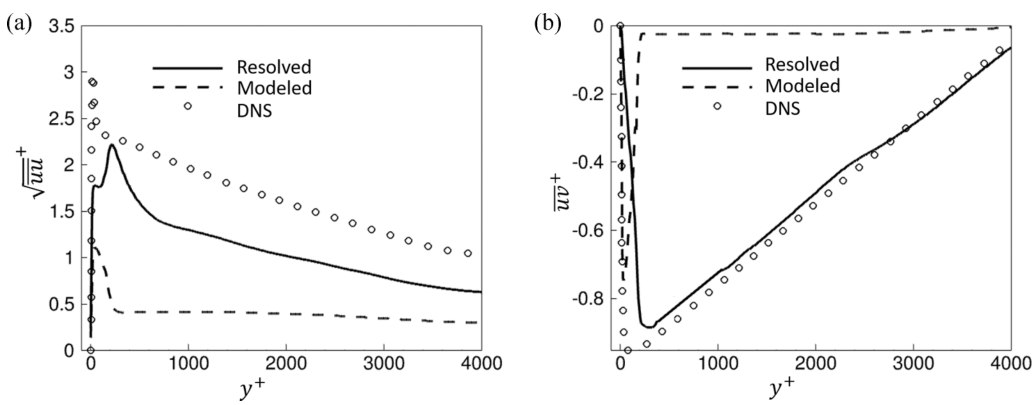

FIG. 13. WM-PANS simulation of turbulent channel for $\mathrm{Re}_\tau = 4200$: (a) Resolved ($\sqrt{\overline{uu}^R}$) and modeled ($\sqrt{\overline{uu}^M}$) streamwise stresses and (b) resolved ($\overline{uv}^R$) and modeled ($\overline{uv}^M$) shear stresses.

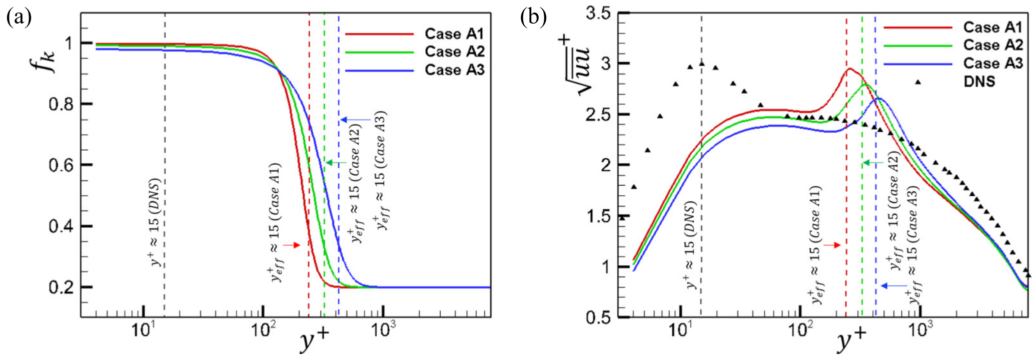

FIG. 14. WM-PANS simulation for $\mathrm{Re}_\tau = 8000$: (a) prescribed f_k variation and (b) profiles of streamwise Reynolds stresses ($\sqrt{\overline{uu}}$). DNS data of Ref. [32] are used for comparison. The results clearly demonstrate that a twitch occurs in the computational buffer layer.

Figure 15 illustrates the fluctuating spanwise vorticity contours (ω_z') in the $x - y$ plane for cases A1 and A3. The contours indicate that the RANS region contains footprints of the unsteadiness from the outer region. However, the intensity of the vortical fluctuations is damped due to the high eddy viscosity in this region and further stabilized by the additional contribution from the positive ν_{Tr}. As the f_k is spatially reduced along the wall-normal direction (y^+), the instabilities are released leading to formation of multiscale turbulence structures in the interior of the channel. It is evident that the resolution of structures is directly dependent on the switchover location. Therefore, this switchover region behaves as a computationally NT/T interface [34]. Across this interface, increase in fluctuating vorticity content is visible as the resolution increases away from the wall and additionally forced by the negative ν_{Tr} in this region. Clearly, the twitch is located at the computational NT/T interface and is a result of a numerical transition.

An important observation is that the structures generated in the computational buffer layer are turbulence like, arising due to reduction in the local total viscosity. As mentioned before, the amount of energy injected through the negative ν_{Tr} is determined by the energy conservation principles. Therefore, a consistent amount of energy is injected into the resolved scales independent of the particular choice of $f_k(y^+)$ as long as the numerical resolution is sufficient.

VI. CONCLUSION

In this paper, near-wall treatment of the PANS-SRS model is developed using spatially varying physical resolution. The commutation residue originating due to the implicit resolution variation

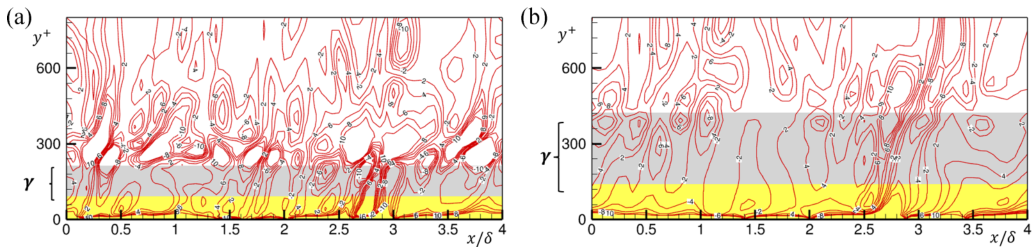

FIG. 15. Spanwise fluctuating vorticity ($\omega_z'\delta/U_c$) contours (red) in *x*-*y* plane for (a) case A1 and (b) case A3 for $\mathrm{Re}_\tau = 8000$. The yellow shaded region is the RANS region, white region is the unsteady PANS region, and the switchover region is denoted by the grey shaded area with width (γ); U_c is the velocity in center of the channel.

is systematically derived based on the energy conservation principles and modeled in terms of a commutation viscosity, ν_{Tr}. Three different near-wall PANS treatments are analyzed: (i) uniform f_k throughout the domain, WR-PANS; (ii) variable f_k without including commutation residue, WOC-PANS; and (iii) variable f_k with the commutation residue model, WM-PANS. WR-PANS requires high numerical resolution for large Reynolds number simulations. WOC-PANS treatment fails to predict right flow statistics as the required energy exchange between scales is not accounted for adequately.

WM-PANS is employed to perform simulations of turbulent channel flow at high Reynolds numbers in the range of $950 \leqslant \mathrm{Re}_\tau \leqslant 8000$. The effect of the flow physics of the computational buffer region on the turbulent flow statistics is evaluated. In addition, the effect of varying the switchover region is thoroughly examined. The results indicate that the log-layer profile and stress components are adequately recovered at all Reynolds numbers and consistent amount energy exchange between the scales is achieved.

In contrary to many other methods where turbulence is injected into the simulation by forcing the solution with artificially generated turbulence, we use a passive method to inject turbulence into the resolved field. To our understanding, the small total viscosity acts together with the natural instability in the computational buffer layer and reinforces the existing turbulence structures with a consistent amount of kinetic energy. Visualization of the turbulence structures in the switchover region as well as energy spectra taken outside the switchover region affirms that turbulence, not just numerical noise, is produced. Hence, the method is cheap, easily implemented, and applicable in general flows. Application of WM-PANS for high-Reynolds number flows in complex geometry is now underway.

ACKNOWLEDGMENTS

Portions of this research were conducted with the advanced computing resources provided by Texas A&M High Performance Research Computing. We would like to thank the reviewers for their valuable suggestions.

APPENDIX A: UNRESOLVED KINETIC ENERGY (k_u) EQUATION

Here, we derive the unresolved kinetic energy (k_u) equation for WM-PANS. Following the methodology proposed in Ref. [14] for uniform-f_k, we begin with the RANS k equation and multiply it with a spatiotemporally varying f_k:

$$f_k\left(\frac{\partial k}{\partial t}+\overline{U_j}\frac{\partial k}{\partial x_j}=P-\beta^* k\omega+\frac{\partial}{\partial x_j}\left[(\nu+\nu_t/\sigma_k)\frac{\partial k}{\partial x_j}\right]\right). \tag{A1}$$

Here, $\overline{U_j}$ is the Reynolds-averaged (or mean) velocity. Applying f_k to each term in the equation, we get

$$f_k\left(\frac{\partial k}{\partial t}+\overline{U_j}\frac{\partial k}{\partial x_j}\right)=f_k(P-\beta^* k\omega)+f_k\left(\frac{\partial}{\partial x_j}\left[(\nu+\nu_t/\sigma_k)\frac{\partial k}{\partial x_j}\right]\right). \tag{A2}$$

The advective term evolves as

$$f_k\left(\frac{\partial k}{\partial t}+\overline{U_j}\frac{\partial k}{\partial x_j}\right)=\frac{\partial k_u}{\partial t}+U_j\frac{\partial k_u}{\partial x_j}-k\left(\frac{\partial f_k}{\partial t}+\overline{U_j}\frac{\partial f_k}{\partial x_j}\right)+(\overline{U_j}-U_j)\frac{\partial k_u}{\partial x_j}, \tag{A3}$$

where the P_{Tr} term is defined as

$$P_{\mathrm{Tr}}\equiv\frac{k_u}{f_k}\left(\frac{\partial f_k}{\partial t}+\overline{U_j}\frac{\partial f_k}{\partial x_j}\right). \tag{A4}$$

Using scaling arguments, it can be shown that the resolved fluctuations do not contribute to SFS transport [14]. Therefore, the final term $(\overline{U_j}-U_j)\frac{\partial k_u}{\partial x_j}$ can be neglected. Further, according to the results of Ref. [13], $\sigma_{ku} = \frac{f_k}{f_\omega}\sigma_{k,\mathrm{RANS}}$. Therefore, we can write ν_t/σ_k as ν_u/σ_{ku}, where $\nu_u = (f_k/f_\omega)\nu_t$. Then, the diffusion term can be written as

$$f_k\left(\frac{\partial}{\partial x_k}\left[\nu_u^*\frac{\partial k}{\partial x_k}\right]\right) = \frac{\partial}{\partial x_k}\left[\nu_u^*\frac{\partial k_u}{\partial x_k}\right] - 2\nu_u^*\frac{\partial k}{\partial x_j}\frac{\partial f_k}{\partial x_j} - \frac{k_u}{f_k}\frac{\partial}{\partial x_j}\left(\nu_u^*\frac{\partial f_k}{\partial x_j}\right), \tag{A5}$$

where $\nu_u^* = \nu + \nu_u/\sigma_{ku}$. This leads to,

$$f_k\left(\frac{\partial}{\partial x_k}\left[\nu_u^*\frac{\partial k}{\partial x_k}\right]\right) = \frac{\partial}{\partial x_k}\left[\nu_u^*\frac{\partial k_u}{\partial x_k}\right] - \frac{2\nu_u^*}{f_k^2}\frac{\partial f_k}{\partial x_j}\left(f_k\frac{\partial k_u}{\partial x_j} - k_u\frac{\partial f_k}{\partial x_j}\right) - \frac{k_u}{f_k}\frac{\partial}{\partial x_j}\left(\nu_u^*\frac{\partial f_k}{\partial x_j}\right). \tag{A6}$$

Therefore, the diffusion term can be written as

$$f_k\left(\frac{\partial}{\partial x_k}\left[\nu_u^*\frac{\partial k}{\partial x_k}\right]\right) = \frac{\partial}{\partial x_k}\left[\nu_u^*\frac{\partial k_u}{\partial x_k}\right] + D_{\mathrm{Tr}}, \tag{A7}$$

where the commutation residue due to the diffusion term is derived as

$$D_{\mathrm{Tr}} \equiv -\frac{k_u}{f_k}\frac{\partial}{\partial x_k}\left(\nu_u^*\frac{\partial f_k}{\partial x_k}\right) - \frac{2\nu_u^*}{f_k}\left(\frac{\partial k_u}{\partial x_k} - \frac{k_u}{f_k}\frac{\partial f_k}{\partial x_k}\right)\frac{\partial f_k}{\partial x_k};\quad \nu_u^* = \nu + \frac{\nu_u}{\sigma_{ku}} \tag{A8}$$

The production, dissipation, and transport terms are modeled according to the framework outlined in Ref. [14]. The final unresolved kinetic energy (k_u) equation is

$$\frac{\partial k_u}{\partial t} + U_j\frac{\partial k_u}{\partial x_j} = P_u - \beta^* k_u\omega_u + P_{\mathrm{Tr}} + D_{\mathrm{Tr}} + \frac{\partial}{\partial x_j}\left[(\nu + \nu_u/\sigma_{ku})\frac{\partial k_u}{\partial x_j}\right]. \tag{A9}$$

APPENDIX B: UNRESOLVED SPECIFIC DISSIPATION RATE (ω_u) EQUATION

The unresolved dissipation rate (ϵ_u) remains unaffected due to spatiotemporal variations of f_k if the cutoff is outside the dissipation range [16]. Therefore, to derive the specific rate of dissipation (ω_u) equation, a transformation from the ϵ_u equation is needed. The unresolved dissipation (ϵ_u) is [14]

$$\frac{\partial \epsilon_u}{\partial t} + U_j\frac{\partial \epsilon_u}{\partial x_j} = C_{e1}\frac{P_u\epsilon_u}{k_u} - C_{e2}^*\frac{\epsilon_u^2}{k_u} + \frac{\partial}{\partial x_j}\left[(\nu + \nu_u/\sigma_{\epsilon u})\frac{\partial \epsilon_u}{\partial x_j}\right]. \tag{B1}$$

Now, using the relation $\epsilon_u = \beta^* k_u\omega_u$, the above equation can be transformed as

$$\frac{\partial \beta^* k_u\omega_u}{\partial t} + U_j\frac{\partial \beta^* k_u\omega_u}{\partial x_j} = C_{e1}\frac{P_u\beta^* k_u\omega_u}{k_u} - C_{e2}^*\frac{(\beta^* k_u\omega_u)^2}{k_u} + \frac{\partial}{\partial x_j}\left[(\nu + \nu_u/\sigma_{\epsilon u})\frac{\partial \beta^* k_u\omega_u}{\partial x_j}\right]. \tag{B2}$$

Simplifying, we get

$$\frac{\partial k_u\omega_u}{\partial t} + U_j\frac{\partial k_u\omega_u}{\partial x_j} = C_{e1}P_u\omega_u - C_{e2}^*\beta^* k_u\omega_u^2 + \frac{\partial}{\partial x_j}\left[(\nu + \nu_u/\sigma_{\epsilon u})\frac{\partial k_u\omega_u}{\partial x_j}\right]. \tag{B3}$$

Assuming $P_{ut} = P_u + P_{Tr} + D_{Tr}$ and adding $-P_{ut}\omega_u + \epsilon_u\omega_u$ to both sides, we can simplify the advective terms on the left-hand side as

$$\frac{\partial k_u\omega_u}{\partial t} + U_j\frac{\partial k_u\omega_u}{\partial x_j} - P_{ut}\omega_u + \epsilon_u\omega_u = k_u\left(\frac{\partial \omega_u}{\partial t} + U_j\frac{\partial \omega_u}{\partial x_j}\right) + \omega_u\left(\frac{\partial k_u}{\partial t} + U_j\frac{\partial k_u}{\partial x_j} - P_{ut} + \epsilon_u\right). \tag{B4}$$

From Eq. (A9), we get

$$\frac{\partial k_u\omega_u}{\partial t} + U_j\frac{\partial k_u\omega_u}{\partial x_j} - P_{ut}\omega_u + \epsilon_u\omega_u = k_u\left(\frac{\partial \omega_u}{\partial t} + U_j\frac{\partial \omega_u}{\partial x_j}\right) + \omega_u\left((\nu + \nu_u/\sigma_{ku})\frac{\partial k_u}{\partial x_j}\right). \tag{B5}$$

Similarly, the transport terms on the right-hand side of Eq. (B3) are simplified as

$$\begin{aligned}\frac{\partial}{\partial x_j}\left[(\nu+\nu_u/\sigma_{\epsilon u})\frac{\partial k_u\omega_u}{\partial x_j}\right] &= \frac{\partial}{\partial x_j}\left[(\nu+\nu_u/\sigma_{\epsilon u})k_u\frac{\partial \omega_u}{\partial x_j}+(\nu+\nu_u/\sigma_{\epsilon u})\omega_u\frac{\partial k_u}{\partial x_j}\right]\\ &= \frac{\partial}{\partial x_j}\left[(\nu+\nu_u/\sigma_{\epsilon u})k_u\frac{\partial \omega_u}{\partial x_j}\right]+\frac{\partial}{\partial x_j}\left[(\nu+\nu_u/\sigma_{\epsilon u})\omega_u\frac{\partial k_u}{\partial x_j}\right]\\ &= 2(\nu+\nu_u/\sigma_{\epsilon u})\frac{\partial k_u}{\partial x_j}\frac{\partial \omega_u}{\partial x_j}+k_u\frac{\partial}{\partial x_j}\left[(\nu+\nu_u/\sigma_{\epsilon u})\frac{\partial \omega_u}{\partial x_j}\right]\\ &\quad+\omega_u\frac{\partial}{\partial x_j}\left[(\nu+\nu_u/\sigma_{\epsilon u})\frac{\partial k_u}{\partial x_j}\right].\end{aligned} \tag{B6}$$

Substituting in Eq. (B3), we get

$$\begin{aligned}k_u\left(\frac{\partial \omega_u}{\partial t}+U_j\frac{\partial \omega_u}{\partial x_j}\right) &= C_{e1}P_u\omega_u - C_{e2}^*\beta^*k_u\omega_u^2 - P_{ut}\omega_u+\beta^*k_u\omega_u\omega_u\\ &\quad+2(\nu+\nu_u/\sigma_{\epsilon u})\frac{\partial k_u}{\partial x_j}\frac{\partial \omega_u}{\partial x_j}+k_u\frac{\partial}{\partial x_j}\left[(\nu+\nu_u/\sigma_{\epsilon u})\frac{\partial \omega_u}{\partial x_j}\right].\end{aligned} \tag{B7}$$

Rearranging the terms in the above equation:

$$\begin{aligned}\frac{\partial \omega_u}{\partial t}+U_j\frac{\partial \omega_u}{\partial x_j} &= (C_{e1}-1)\frac{P_u\omega_u}{k_u}-\frac{(P_{\mathrm{Tr}}+D_{\mathrm{Tr}})\omega_u}{k_u}-(C_{e2}^*-1)\beta^*\omega_u^2\\ &\quad+\frac{\partial}{\partial x_j}\left[(\nu+\nu_u/\sigma_{\epsilon u})\frac{\partial \omega_u}{\partial x_j}\right]+\frac{2}{k_u}(\nu+\nu_u/\sigma_{\epsilon u})\frac{\partial k_u}{\partial x_j}\frac{\partial \omega_u}{\partial x_j}.\end{aligned} \tag{B8}$$

The additional term arising due to spatial variation of f_k in the ω_u equation is $D_{\mathrm{Tr}\omega} = -(P_{Tr}+D_{Tr})\omega_u/\,k_u$. Therefore, the final ω_u equation in the PANS $k_u-\omega_u$ model [30] is modified as

$$\frac{\partial \omega_u}{\partial t}+U_j\frac{\partial \omega_u}{\partial x_j}=\alpha\frac{P_u\omega_u}{k_u}+D_{\mathrm{Tr}\omega}-\beta'\omega_u^2+\frac{\partial}{\partial x_j}\left[(\nu+\nu_u/\sigma_{\omega u})\frac{\partial \omega_u}{\partial x_j}\right]. \tag{B9}$$

---

[1] P. R. Spalart, W.-H. Jou, M. Strelets, and S. R. Allmaras, Comments on the feasibility of LES for wings, and on a hybrid RANS/LES approach, in *Proceedings of first AFOSR international conference on DNS/LES, Ruston, Louisiana* (Greyden Press, 1997).

[2] D. C. Wilcox, *Turbulence Modeling for CFD* (DCW industries La Canada, CA, 1998), Vol. 1

[3] U. Piomelli and E. Balaras, Wall-layer models for large-eddy simulations, Annu. Rev. Fluid Mech. **34**, 349 (2002).

[4] S. Kawai and J. Larsson, Wall-modeling in large eddy simulation: Length scales, grid resolution, and accuracy, Phys. Fluids **24**, 015105 (2012).

[5] S. T. Bose and G. I. Park, Wall-modeled large-eddy simulation for complex turbulent flows, Annu. Rev. Fluid Mech. **50**, 535 (2018).

[6] M. Wang and P. Moin, Dynamic wall modeling for large-eddy simulation of complex turbulent flows, Phys. Fluids **14**, 2043 (2002).

[7] X. I. Yang and S. T. Bose, A physical basis of the slip-wall model for wall-modeled large-eddy simulations, in *10th International Symposium on Turbulence and Shear Flow Phenomena (TSFP10)* (Chicago, USA, 2017).

[8] P. R. Spalart, Detached-eddy simulation, Ann. Rev. Fluid Mech. **41**, 181 (2009).

[9] S. Deck, Zonal-detached-eddy simulation of the flow around a high-lift configuration, AIAA J. **43**, 2372 (2005).

[10] C. Speziale, Turbulence modeling for time-dependent RANS and VLES: A review, AIAA J. **36**, 173 (1998).

[11] S. Girimaji and K. Abdol-Hamid, Partially-averaged Navier Stokes model for turbulence: Implementation and validation, *In 43rd AIAA Aerospace Sciences Meeting and Exhibit, Reno, Nevada* (AIAA, Reston, VA, 2005).

[12] B. Chaouat and R. Schiestel, A new partially integrated transport model for subgrid-scale stresses and dissipation rate for turbulent developing flows, Phys. Fluids **17**, 065106 (2005).

[13] P. Tazraei and S. S. Girimaji, Scale-resolving simulations of turbulence: Equilibrium boundary layer analysis leading to near-wall closure modeling, Phys. Rev. Fluids **4**, 104607 (2019).

[14] S. S. Girimaji, Partially-averaged Navier-Stokes model for turbulence: A Reynolds-averaged Navier-Stokes to direct numerical simulation bridging method, J. Appl. Mech. **73**, 413 (2006).

[15] M. Germano, Turbulence: the filtering approach, J. Fluid Mech. **238**, 325 (1992).

[16] S. S. Girimaji and S. Wallin, Closure modeling in bridging regions of variable-resolution (VR) turbulence computations, J. Turbul. **14**, 72 (2013).

[17] S. Wallin and S. Girimaji, Commutation error mitigation in variable-resolution pans closure: Proof of concept in decaying isotropic turbulence, in *6th AIAA Theoretical Fluid Mechanics Conference, Honululu, Hawaii* (AIAA, Reston, VA, 2011).

[18] S. Lakshmipathy and S. S. Girimaji, Partially averaged Navier-Stokes (pans) method for turbulence simulations: Flow past a circular cylinder, J. Fluids Eng. **132**, 121202 (2010).

[19] D. A. Reyes, J. M. Cooper, and S. S. Girimaji, Characterizing velocity fluctuations in partially resolved turbulence simulations, Phys. Fluids **26**, 085106 (2014).

[20] P. Razi, P. Tazraei, and S. Girimaji, Partially-averaged Navier–Stokes (PANS) simulations of flow separation over smooth curved surfaces, Int. J. Heat Fluid Flow **66**, 157 (2017).

[21] F. S. Pereira, L. Eça, G. Vaz, and S. S. Girimaji, Challenges in scale-resolving simulations of turbulent wake flows with coherent structures, J. Comput. Phys. **363**, 98 (2018).

[22] B. Basara, S. Krajnović, and S. Girimaji, PANS vs. LES for computations of the flow around a 3D bluff body, in *2nd International Conference on Turbulence and Interaction* (Martinique, France, 2009).

[23] A. Frendi, A. Tosh, and S. Girimaji, Flow past a backward-facing step: Comparison of PANS, DES and URANS results with experiments, Int. J. Comput. Methods Eng. Sci. Mech. **8**, 23 (2006).

[24] C. Kamble, S. S. Girimaji, and H.-C. Chen, Partially averaged Navier-Stokes formulation of a two-layer turbulence model, AIAA J. **58**, 174 (2020).

[25] P. Tazraei and S. S. Girimaji, Scale-resolving simulations of spatially evolving turbulence: Physically consistent inflow specification of unresolved velocity and length-scale profiles, Phys. Rev. Fluids **5**, 124604 (2020).

[26] C. Kamble and S. Girimaji, Characterization of coherent structures in turbulent wake of a sphere using partially averaged Navier—Stokes (PANS) simulations, Phys. Fluids **32**, 105110 (2020).

[27] J. Zhang, G. Minelli, A. N. Rao, B. Basara, R. Bensow, and S. Krajnović, Comparison of PANS and LES of the flow past a generic ship, Ocean Eng. **165**, 221 (2018).

[28] A. Rao, G. Minelli, B. Basara, and S. Krajnović, On the two flow states in the wake of a hatchback ahmed body, J. Wind Eng. Ind. Aerodyn. **173**, 262 (2018).

[29] G. Minelli, S. Krajnović, and B. Basara, A flow control study of a simplified, oscillating truck cabin using PANS, J. Fluids Eng. **140**, 121101 (2018).

[30] S. Lakshmipathy and S. S. Girimaji, Partially-averaged Navier-Stokes method for turbulent flows: $k-\omega$ model implementation, in *Collection of Technical Papers - 44th AIAA Aerospace Sciences Meeting and Exhibit, Reno, Nevada* (AIAA, Reston, VA, 2006).

[31] F. R. Menter, Two-equation eddy-viscosity turbulence models for engineering applications, AIAA J. **32**, 1598 (1994).

[32] Y. Yamamoto and Y. Tsuji, Numerical evidence of logarithmic regions in channel flow at $\mathrm{re}_\tau = 8000$, Phys. Rev. Fluids **3**, 012602(R) (2018).

[33] J. Larsson, F. Lien, and E. Yee, The artificial buffer layer and the effects of forcing in hybrid LES/RANS, Int. J. Heat Fluid Flow **28**, 1443 (2007).

[34] C. B. da Silva, J. C. Hunt, I. Eames, and J. Westerweel, Interfacial layers between regions of different turbulence intensity, Annu. Rev. Fluid Mech. **46**, 567 (2014).
[35] D. K. Bisset, J. C. R. Hunt, and M. M. Rogers, The turbulent/non-turbulent interface bounding a far wake, J. Fluid Mech. **451**, 383 (2002).
[36] H. Jasak, A. Jemcov, and Z. Tukovic, Openfoam: A c++ library for complex physics simulations, in *International Workshop on Coupled Methods in Numerical Dynamics* (2007), Vol. 1000, pp. 1–20.
[37] R. I. Issa, Solution of the implicitly discretised fluid flow equations by operator-splitting, J. Comput. Phys. **62**, 40 (1986).
[38] P. Razi, Partially-averaged Navier-Stokes (PANS) method for turbulence simulations: Near-wall modeling and smooth-surface separation computations, arXiv:1712.03796.
[39] S. Hoyas and J. Jiménez, Reynolds number effects on the Reynolds-stress budgets in turbulent channels, Phys. Fluids **20**, 101511 (2008).
[40] J. Kim, P. Moin, and R. Moser, Turbulence statistics in fully developed channel flow at low Reynolds number, J. Fluid Mech. **177**, 133 (1987).